CrossMark

Actively tunable broadband terahertz absorption using periodically square-patterned graphene

Longfang Ye[1,2]*, Xin Chen[1], Jianliang Zhuo[1], Feng Han[1], and Qing Huo Liu[3]

[1]*Institute of Electromagnetics and Acoustics, and Department of Electronic Science, Xiamen University, Xiamen 361005, China*
[2]*Shenzhen Research Institute of Xiamen University, Shenzhen 518057, China*
[3]*Department of Electrical and Computer Engineering, Duke University, Durham, NC 27708, U.S.A.*

*E-mail: lfye@xmu.edu.cn

We propose an actively tunable broadband perfect absorber using a square-patterned graphene–spacer–polysilicon–spacer–metal structure. The simulated results show that the absorber can reach nearly perfect broadband terahertz absorption with over 99.5% (90%) absorbance from 1.52 (1.27) to 2.23 (2.51) THz, corresponding to the normalized bandwidth of 37.5% (65.6%) under normal incidence with the graphene Fermi level of 0.7 eV. The absorption spectra show a clear independence of the polarization and the angle of incidence. By adjusting the graphene Fermi level from 0 to 0.7 eV, the peak absorbance can be continuously tuned from 15 to 100% without shifting the absorption frequency band. © 2018 The Japan Society of Applied Physics

Terahertz (THz) radiation, with the frequency ranging from 0.1 to 10 THz, has extensive applications including sensing, imaging, spectroscopy, and communications.[1–3] As one variety of key devices, terahertz absorbers have attracted increasing attention in recent years. Since the first metamaterial absorber was proposed by Landy et al. in 2008,[4] various metamaterial absorbers have been explored.[5,6] A tunable metamaterial absorber is an optical device capable of adjusting dynamically its absorption property in a controllable manner. To make the conventionally fixed metamaterial absorbers tunable, some tunable elements or tunable materials, such as PIN diodes,[7] MEMS switches,[8] varactors,[9] liquid crystals,[10] and graphene,[11] have been applied in metamaterial structures. Owing to its excellent electromagnetic property and tunability via chemical or electrostatic doping, graphene has become one of the most promising materials for novel tunable terahertz optoelectronic devices such as modulators, biosensors, and absorbers.[12–17] Graphene is an atom-thick two-dimensional material with very low absorption (∼2.3%) at normal incidence from infrared to the visible range.[18] Recently, to enhance the absorption and modulation depth, various graphene-based absorbers with periodically separated graphene disk, ribbon, and ring arrays,[17,19–21] grating-incorporated structures,[22] and hybrid metamaterial structures[23] have been investigated. To further broaden absorption bandwidth, many graphene-based absorbers with graphene fishnet metamaterial,[24] graphene multiresonators, and multilayered graphene structures have also been proposed.[25,26] However, many of these absorbers suffer from some drawbacks, such as absorption tuning difficulties via graphene electrostatic biasing for the separated graphene units or polarization/angle dependence, which greatly restrict their practical applications. Therefore, the effective design of a perfect metamaterial absorber with broadband, wide-angle, polarization-independent, and strong tunability is highly desirable for emerging terahertz applications.

In this letter, we propose a promising actively tunable broadband terahertz metamaterial absorber using a periodically square-patterned electric-continuous graphene array with advantages of wider bandwidth of perfect absorption, larger absorption modulation, and more convenience in electrostatic biasing than conventional graphene-based absorbers.
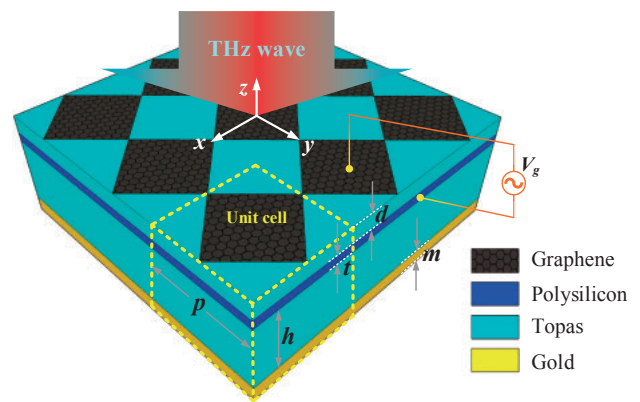
Fig. 1. Schematic of the proposed actively tunable broadband graphene-based terahertz absorber, where the parameters are set as $p = 40\,\mu m$, $d = t = 20\,nm$, $h = 27\,\mu m$, and $m = 0.5\,\mu m$.

Below, we study the structure design and properties of this absorber, including absorption spectra, retrieved effective impedance, field distributions, absorbance tunability, and dependences of the polarization and angle of incidence.

The schematic of the proposed actively tunable broadband terahertz absorber is depicted in Fig. 1. The periodically square-patterned graphene layer is on top of the absorber, placed on the multilayered spacer/polysilicon/spacer/metal structure. The four corners of each square-patterned graphene unit are connected to achieve an electrically continuous graphene layer. The polysilicon layer with a relative permittivity (ε_g) of 3 acts as an electrostatic gating layer of graphene for absorption tuning. The spacer layers are assumed as a polyethylene cyclic olefin copolymer (Topas) with a relative permittivity (ε_d) of 2.35, and the bottom metal layer is modeled as gold using the Drude model.[15,24,27] The graphene is modeled as an infinitely thin layer with 2D surface conductivity $\sigma_g(\omega, \mu_c, \tau, T)$ determined using the Kubo formula,[28] where ω is the radian frequency, μ_c is the Fermi level, τ is the relaxation time, and T is the temperature. We assume $\tau = 0.1\,ps$, a reasonable value according to Ref. 17, and $T = 300\,K$. The unit cell period of the proposed absorber is p in both x- and y-directions, and the thicknesses of the upper Topas spacer, polysilicon, lower Topas spacer, and metal layer are d, t, h, and m, respectively. The dimensional param-
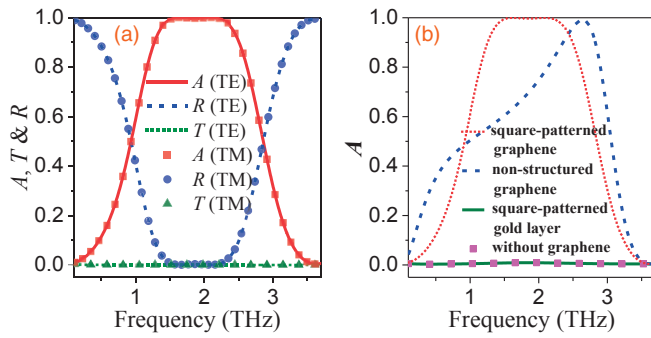
Fig. 2. (a) Simulated reflection (R), transmission (T), and absorbance (A) of the proposed absorbers with square-patterned graphene at $\mu_c = 0.7\,\text{eV}$ for both TE and TM polarizations under normal terahertz incidence. (b) Simulated absorbance for the absorber structures with square-patterned graphene, nonstructured graphene, and square-patterned gold, and without graphene on top for both TE and TM polarizations at normal incidence, where $\mu_c = 0.7\,\text{eV}$ and the dimensional parameters are the same as those shown in Fig. 1.

eters are set as $p = 40\,\mu\text{m}$, $d = 20\,\text{nm}$, $t = 20\,\text{nm}$, $h = 26.96\,\mu\text{m}$, and $m = 0.5\,\mu\text{m}$. In the numerical simulations, the periodic boundaries in both x- and y-directions and Floquet ports in the z-direction are assigned to the absorber unit cell. The absorbance of the absorber can be obtained as $A(\omega) = 1 - T(\omega) - R(\omega)$, where the transmission $T(\omega)$ is equal to $|S_{21}|^2$ and the reflectance $R(\omega)$ is equal to $|S_{11}|^2$.[4,17] In addition, it should be pointed out that, because the thickness of the gating layer is very small with respect to the total thickness of the device, a moderate relative permittivity change, such as that observed using silicon ($\varepsilon_{\text{silicon}} = 11.68$) instead of polysilicon, will only have a negligible effect on the absorbance of the absorber.

Here, we first investigate the absorption properties of the proposed absorber with $\mu_c = 0.7\,\text{eV}$ under normal incidence. Figure 2(a) shows the absorbance A, reflectance R, and transmission T for TE- and TM-polarized incident THz waves. The results show that the absorber can reach nearly perfect broadband terahertz absorption with over 99.5% (90%) ab-

sorbance from 1.52 (1.27) to 2.23 (2.51) THz, corresponding to the normalized bandwidth of 37.5% (65%) for both TE and TM polarizations. The absolute polarization independence is also observed owing to its symmetrical square-patterned graphene structure. Figure 2(b) shows an absorbance comparison among the absorber structures with square-patterned graphene, nonstructured graphene, and square-patterned gold, and without graphene on top for both TE and TM polarizations at normal incidence under the identical dimensional parameters shown in Fig. 1. The proposed absorber demonstrates a symmetric, flat-top absorbance spectrum with a significantly wider bandwidth of 90% absorbance than the structure with a nonstructured graphene layer. Both the structure utilizing a square-patterned gold layer instead of a square-patterned graphene layer and the structure without a graphene layer actually act as perfect reflectors with absorbances very close to 0. Therefore, the square-patterned graphene layer plays a major role in enhancing the bandwidth and absorbance of the absorber.

To better understand the mechanism of the proposed absorber, the electric field distributions, losses in different materials, and effective impedance of the absorber are presented in Fig. 3. The normalized electric field distributions for the TE and TM polarizations on the patterned graphene layer (xoy plane) at 2 and 0.1 THz are depicted in Figs. 3(a)–3(b) and 3(c)–3(d), respectively. It is observed that extremely confined electric fields are distributed around the edges of the square-patterned graphene layer at 2 THz, resulting in a strong terahertz absorption. On the other hand, there are very tiny electric fields distributed on the graphene layer at 0.1 THz for both polarizations. These field distributions agree well with the near-unity and near-zero absorbances of the absorption spectra at 2 and 0.1 THz, respectively. Because of the symmetric structure of the absorber, the electric field distribution of the TM polarization is exactly the same as that of the TE polarization with 90° rotation, leading to the same absorption properties for TE- and TM-polarized waves. Figure 3(e) shows the simulated loss in each material of the absorber. The results reveal that almost all the terahertz
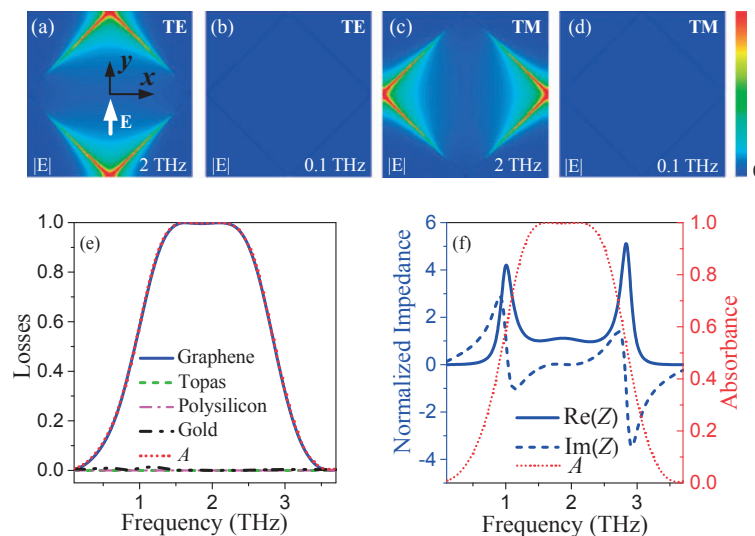
Fig. 3. (a)–(d) Normalized electric field distributions for TE- and TM-polarized terahertz waves at 0.1 and 2 THz, respectively. (e) Losses in different materials of the absorber. (f) Retrieved effective impedance (Z) of the proposed absorbers, where the blue solid, blue dashed, and red dotted curves represent Re(Z), Im(Z), and A, respectively.
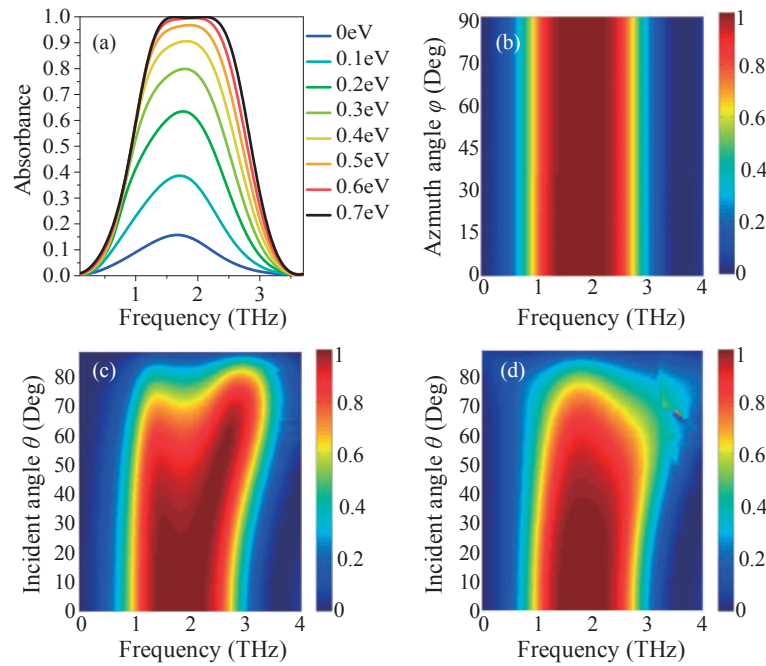
Fig. 4. (a) Absorption spectra of the absorber for both TE and TM polarizations with different μ_c values. (b) Dependence of absorption spectra on polarization angle φ under normal incidence. (c, d) Dependences of absorbance on the angle of incidence (θ) for TE and TM polarizations, respectively.

energy is dissipated as a surface loss within the graphene layer. By assuming Topas and polysilicon as lossless materials, there is no energy dissipated in both of them, and only the remaining negligible energy is dissipated as a volume loss within the gold ground layer. The physical origin of this absorption phenomenon can be interpreted through the effective medium theory.[29] The effective impedance Z of the proposed graphene perfect absorber can be retrieved from the complex frequency-dependent S_{11} and S_{21}, as shown in Fig. 3(f), where the blue solid and dashed curves indicate the real and imaginary parts of Z, respectively. It is found that the effective impedance Z matches the free space impedance with Re(Z) close to 1 and Im(Z) close to 0 in a wide frequency band ranging from 1.52 to 2.23 THz (corresponding to absorption bandwidth). The thick gold plate suppresses the transmission of all the incident terahertz waves. Therefore, together with a small reflectance and the absence of the transmission of the absorber, a broadband absorption with high absorbance is achieved.

The active absorbance tunability of the proposed broadband terahertz absorber and the dependence of absorbance on the polarization angle and the angle of incidence are further studied. Figure 4(a) shows the absorbance A as a function of the frequency f and μ_c for TE and TM polarizations under normal terahertz incidence. It is observed that the peak absorbance continually increases from 15 to 100% while maintaining the same operating bandwidth characteristics as μ_c increases from 0 to 0.7 eV by changing the gate voltage V, demonstrating excellent broadband terahertz absorption modulation above 85%. Therefore, such an actively tunable absorber with a large modulation ability can be applied as a terahertz broadband attenuator, filter, reflector or spatial modulator. Figure 4(b) depicts the dependence of the absorbance A on the frequency f and the polarization angle φ ranging from 0 to 90° under normal incidence. With increasing φ, the absorption property is completely unchanged. This absolute polarization independence results from the axisymmetric

structure, which is of great value for extending its application scenario. The characteristics of the proposed absorber under the oblique terahertz incidence case are also investigated. Figures 4(c) and 4(d) show the dependences of the absorbance on the angle of incidence (θ) for both TE and TM polarizations, respectively. The designed absorber demonstrates prominent absorption performance with stable broadband absorbance over a wide range of angles of incidence. It is observed that the broadband absorbance above 80% from 1.48 to 2.41 THz for both TE and TM polarizations is still achieved even at $\theta = 60°$. However, note that as θ increases, the peak absorbance for TM polarization decreases rapidly, while that for TE polarization decreases slightly even for θ values larger than 60°. The different behaviors can be interpreted by the electric-dipole-like plasmonic resonances of the absorber. With increasing θ, the tangential electric field of the TM polarization decreases accordingly, but that of the TE polarization remains constant. Nevertheless, this actively tunable absorber with excellent modulation capability and independence of the polarization angle and angle of incidence may have great potential for diverse terahertz applications.

In summary, we have demonstrated an active tunable broadband terahertz absorber using periodically square-patterned graphene. The numerical results show that the absorber has an excellent broadband terahertz absorption property with over 99.5% (90%) absorbance from 1.52 (1.27) to 2.23 (2.51) THz for both TE and TM polarizations, demonstrating a clear independence of the polarization and the angle of incidence. The absorbance modulation above 85% with peak absorbance continually tuning from 15 to 100% can be obtained by adjusting the graphene Fermi level from 0 to 0.7 eV while maintaining the operating bandwidth. Owing to the excellent modulation capability and independence of the polarization angle and the angle of incidence, the proposed absorber may be engineered for various actively tunable terahertz filters, attenuators, modulators, reflectors, and other optoelectronic devices.

1) M. Tonouchi, Nat. Photonics **1**, 97 (2007).
2) H. Shigekawa, S. Yoshida, and O. Takeuchi, Nat. Photonics **8**, 815 (2014).
3) J. Federici and L. Moeller, J. Appl. Phys. **107**, 111101 (2010).
4) N. I. Landy, S. Sajuyigbe, J. J. Mock, D. R. Smith, and W. J. Padilla, Phys. Rev. Lett. **100**, 207402 (2008).
5) C. M. Watts, X. Liu, and W. J. Padilla, Adv. Mater. **24**, OP98 (2012).
6) S. Ogawa and M. Kimata, Materials **11**, 458 (2018).
7) D. Lee, H. Jeong, and S. Lim, Sci. Rep. **7**, 4891 (2017).
8) P. Pitchappa, C. P. Ho, P. Kropelnicki, N. Singh, D. Kwong, and C. Lee, Appl. Phys. Lett. **104**, 201114 (2014).
9) J. Zhao, Q. Cheng, J. Chen, M. Qi, W. Jiang, and T. Cui, New J. Phys. **15**, 043049 (2013).
10) D. Shrekenhamer, W. Chen, and W. J. Padilla, Phys. Rev. Lett. **110**, 177403 (2013).
11) Z. Fang, Y. Wang, A. E. Schlather, Z. Liu, P. M. Ajayan, F. J. García de Abajo, P. Nordlander, X. Zhu, and N. J. Halas, Nano Lett. **14**, 299 (2014).
12) A. N. Grigorenko, M. Polini, and K. S. Novoselov, Nat. Photonics **6**, 749 (2012).
13) F. H. Koppens, D. E. Chang, and F. J. García de Abajo, Nano Lett. **11**, 3370 (2011).
14) M. Liu, X. Yin, E. Ulin-Avila, B. Geng, T. Zentgraf, L. Ju, F. Wang, and X. Zhang, Nature **474**, 64 (2011).
15) L. Ye, K. Sui, Y. Liu, M. Zhang, and Q. Liu, Opt. Express **26**, 15935 (2018).
16) D. Rodrigo, O. Limaj, D. Janner, D. Etezadi, F. J. García de Abajo, V. Pruneri, and H. Altug, Science **349**, 165 (2015).
17) S. Thongrattanasiri, F. H. Koppens, and F. J. García de Abajo, Phys. Rev. Lett. **108**, 047401 (2012).
18) R. R. Nair, P. Blake, A. N. Grigorenko, K. S. Novoselov, T. J. Booth, T. Stauber, N. M. R. Peres, and A. K. Geim, Science **320**, 1308 (2008).
19) P. Chen and A. Alu, IEEE Trans. Terahertz Sci. Technol. **3**, 748 (2013).
20) R. Alaee, M. Farhat, C. Rockstuhl, and F. Lederer, Opt. Express **20**, 28017 (2012).
21) S. Xiao, T. Wang, Y. Liu, C. Xu, X. Han, and X. Yan, Phys. Chem. Chem. Phys. **18**, 26661 (2016).
22) X. Zou, G. Zheng, J. Cong, L. Xu, Y. Chen, and M. Lai, Opt. Lett. **43**, 46 (2018).
23) L. Wang, S. Ge, W. Hu, M. Nakajima, and Y. Lu, Opt. Express **25**, 23873 (2017).
24) A. Andryieuski and A. V. Lavrinenko, Opt. Express **21**, 9144 (2013).
25) S. Yi, M. Zhou, X. Shi, Q. Gan, J. Zi, and Z. Yu, Opt. Express **23**, 10081 (2015).
26) M. Amin, M. Farhat, and H. Bağcı, Opt. Express **21**, 29938 (2013).
27) P. D. Cunningham, N. N. Valdes, F. A. Vallejo, L. M. Hayden, B. Polishak, X. H. Zhou, and R. J. Twieg, J. Appl. Phys. **109**, 043505 (2011).
28) G. W. Hanson, J. Appl. Phys. **103**, 064302 (2008).
29) D. R. Smith, D. C. Vier, T. Koschny, and C. M. Soukoulis, Phys. Rev. E **71**, 036617 (2005).